J|A|C|S
ARTICLES
Published on Web 10/26/2002

Mössbauer Quadrupole Splittings and Electronic Structure in Heme Proteins and Model Systems: A Density Functional Theory Investigation

Yong Zhang, Junhong Mao, Nathalie Godbout, and Eric Oldfield*

Contribution from the Department of Chemistry, University of Illinois at Urbana-Champaign, 600 South Mathews Avenue, Urbana, Illinois 61801

Received February 26, 2002. Revised Manuscript Received August 21, 2002

Abstract: We report the results of a series of density functional theory (DFT) calculations aimed at predicting the ^{57}Fe Mössbauer electric field gradient (EFG) tensors (quadrupole splittings and asymmetry parameters) and their orientations in $S = 0$, $^1/_2$, 1, $^3/_2$, 2, and $^5/_2$ metalloproteins and/or model systems. Excellent results were found by using a Wachter's all electron basis set for iron, 6-311G* for other heavy atoms, and 6-31G* for hydrogen atoms, BPW91 and B3LYP exchange-correlation functionals, and spin-unrestricted methods for the paramagnetic systems. For the theory versus experiment correlation, we found $R^2 = 0.975$, slope $= 0.99$, intercept $= -0.08$ mm sec^{-1}, rmsd $= 0.30$ mm sec^{-1} ($N = 23$ points) covering a ΔE_Q range of 5.63 mm s^{-1} when using the BPW91 functional and $R^2 = 0.978$, slope $= 1.12$, intercept $= -0.26$ mm sec^{-1}, rmsd $= 0.31$ mm sec^{-1} when using the B3LYP functional. ΔE_Q values in the following systems were successfully predicted: (1) ferric low-spin ($S = ^1/_2$) systems, including one iron porphyrin with the usual $(d_{xy})^2(d_{xz}d_{yz})^3$ electronic configuration and two iron porphyrins with the more unusual $(d_{xz}d_{yz})^4(d_{xy})^1$ electronic configuration; (2) ferrous NO-heme model compounds ($S = ^1/_2$); (3) ferrous intermediate spin ($S = 1$) tetraphenylporphinato iron(II); (4) a ferric intermediate spin ($S = ^3/_2$) iron porphyrin; (5) ferrous high-spin ($S = 2$) deoxymyoglobin and deoxyhemoglobin; and (6) ferric high spin ($S = ^5/_2$) metmyoglobin plus two five-coordinate and one six-coordinate iron porphyrins. In addition, seven diamagnetic ($S = 0$, d^6 and d^8) systems studied previously were reinvestigated using the same functionals and basis set scheme as used for the paramagnetic systems. All computed asymmetry parameters were found to be in good agreement with the available experimental data as were the electric field gradient tensor orientations. In addition, we investigated the electronic structures of several systems, including the $(d_{xy})^2(d_{xz},d_{yz})^3$ and $(d_{xz},d_{yz})^4(d_{xy})^1$ [Fe(III)/porphyrinate]$^+$ cations as well as the NO adduct of Fe(II)(octaethylporphinate), where interesting information on the spin density distributions can be readily obtained from the computed wave functions.

Introduction

The nature of metal−ligand bonding in heme proteins has been the topic of lively debate for several decades.[1−5] Part of the debate often focuses on how small molecule ligands, such as CO, O_2, NO, CN^-, N_3^-, H_2O, and so forth bind to the iron site. Here, X-ray crystallography is the most widely used technique to derive structural information.[6−10] However, when local as opposed to more global structural information is of interest, then other spectroscopic methods can play a role and in fact may be even more suitable for probing how, for example, small molecules such as CO bind to Fe.[11−13] For example, in recent work, we used a combination of ^{13}C NMR, ^{17}O NMR, ^{57}Fe NMR, ^{57}Fe Mössbauer, and IR spectroscopies to investigate CO binding to myoglobin. By using density functional theory (DFT) to make correlations between the spectroscopic observables and structure, we concluded that CO bound with a tilt $\tau = 4°$ and a bend $\beta = 7°$ (for the A_1 substate).[11] This result was subsequently confirmed by a high-resolution synchrotron X-ray structure determination[6] which found $\tau = 4.7°$ and $\beta = 7.4°$.

The CO- and O_2-bonded heme proteins we investigated were, however, diamagnetic, and many interesting metalloproteins are

* Address correspondence to this author. E-mail: eo@chad.scs.uiuc.edu.

(1) Pauling, L. *Nature* **1964**, *203*, 182−183.
(2) Weiss, J. *Nature* **1964**, *203*, 183.
(3) Park, K. D.; Guo, K.; Adebodun, F.; Chiu, M. L.; Sligar, S. G.; Oldfield, E. *Biochemistry* **1991**, *30*, 2333−2347.
(4) Ray, G. B.; Li, Z.-Y.; Ibers, J. A.; Sessler, J. L.; Spiro, T. G. *J. Am. Chem. Soc.* **1994**, *116*, 162−176.
(5) Lim, M.; Jackson, T. A.; Anfinrud, P. A. *Science* **1995**, *269*, 962−966.
(6) Kachalova, G. S.; Popov, A. N.; Bartunik, H. D. *Science* **1999**, *284*, 475−476.
(7) Zhang, J.; Hua, Z.; Tame, J. R.; Lu, G.; Zhang, R.; Gu, X. *J. Mol. Biol.* **1996**, *255*, 484−493.
(8) Brucker, E. A.; Olson, J. S.; Ikeda-Saito, M.; Phillips, G. N. *Proteins: Struct., Funct., Genet.* **1998**, *30*, 352−356.
(9) Bolognesi, M.; Rosano, C.; Losso, R.; Borassi, A.; Rizzi, M.; Wittenberg, J. B.; Boffi, A.; Ascenzi, P. *Biophys. J.* **1999**, *77*, 1093−1099.
(10) Lionetti, C.; Guanziroli, M. G.; Frigerio, F.; Ascenzi, P.; Bolognesi, M. *J. Mol. Biol.* **1991**, *217*, 409−412.
(11) McMahon, M.; deDios, A. C.; Godbout, N.; Salzmann, R.; Laws, D. D.; Le, H.; Havlin, R. H.; Oldfield, E. *J. Am. Chem. Soc.* **1998**, *120*, 4784−4797.
(12) Godbout, N.; Havlin, R.; Salzmann, R.; Debrunner, P. G.; Oldfield, E. *J. Phys. Chem. A* **1998**, *102*, 2342−2350.
(13) Havlin, R. H.; Godbout, N.; Salzmann, R.; Wojdelski, M.; Arnold, W.; Schulz, C. E.; Oldfield, E. *J. Am. Chem. Soc.* **1998**, *120*, 3144−3151.

paramagnetic. There is considerable spectroscopic information on, for example, the Mössbauer electric field gradients (the quadrupole splittings, ΔE_Q, and the electric field gradient (EFG) tensor asymmetry parameters, η) on paramagnetic systems in the literature[14−19] together with IR,[20−24] electron spin resonance (ESR),[15,25−27] and NMR hyperfine shifts[15,28−32] in paramagnetic proteins and model systems. It would, therefore, clearly be of interest to be able to predict at least some of these parameters theoretically, since then structural−spectroscopic correlations could be made on paramagnetic systems in much the same way as we investigated the topic of CO−heme bonding, leading to local structure predictions/refinements and the confidence to carry out more in-depth studies about electronic structure.

In previous work, there have been a number of reports of the calculation of Mössbauer spectroscopic observables.[33−35] However, it is not clear how general these methods are. For example, can they predict the Mössbauer ΔE_Q observables in all $S = 0$, $^1/_2$, 1, $^3/_2$, 2, and $^5/_2$ spin states? What about the asymmetry parameters? Can the methods used to predict Mössbauer results also be applied to predicting NMR contact shifts (spin densities, $\rho_{\alpha\beta}$)? What about hyperfine interactions in ESR?

In this paper, we investigate some of these questions by computing Mössbauer EFG parameters in both diamagnetic and paramagnetic heme proteins and model systems. Unlike earlier studies, we investigated a relatively large number of paramagnetic molecules (16 structures) chosen to be representative of the possible spin states ($S = ^1/_2$, 1, $^3/_2$, 2, and $^5/_2$) in addition to seven diamagnetic systems, which for the first time covers a Mössbauer ΔE_Q range as large as ~6 mm sec^{-1}. No empirical parameters were used. In addition, we use the results obtained to investigate the electronic structures (spin densities) in several interesting $S = ^1/_2$ metalloporphyrins having different ground states, together with an analysis of the bonding in an NO metalloporphyrin adduct.

Experimental Section

The Mössbauer quadrupole splitting is related to the components of the electric field gradient tensor at the nucleus as follows:[14]

$$\Delta E_Q = \frac{1}{2} eQV_{zz}\left(1 + \frac{\eta^2}{3}\right)^{1/2} \quad (1)$$

where e is the electron charge, Q is the quadrupole moment of the $E^* = 14.4$ keV excited state, and the principal components of the EFG tensor are labeled according to the convention:

$$|V_{zz}| > |V_{yy}| > |V_{xx}| \quad (2)$$

with the asymmetry parameter being given by

$$\eta = \frac{V_{xx} - V_{yy}}{V_{zz}} \quad (3)$$

In this work, we used the Gaussian-98 program[36] to compute the complete electric field gradient tensor at iron. After diagonalization, one obtains the principal components of the traceless second rank tensor: V_{xx}, V_{yy}, and V_{zz}. To obtain the quadrupole splitting, ΔE_Q, all that is needed is the value for V_{zz} plus Q, the quadrupole moment of the ^{57}Fe I* $= ^3/_2$ excited state. Over the years, there has been considerable uncertainty as to the exact value of Q, ranging from -0.19×10^{-28} to $+0.44 \times 10^{-28}$ m^2.[37] Fortunately, this topic was reinvestigated in great detail recently.[37,38] The most precise determination[38] of $Q = 0.16(\pm 5\%) \times 10^{-28}$ was previously found by us to permit excellent predictions of experimental ΔE_Q values for a variety of diamagnetic organometallic complexes, hemes, and heme model compounds,[12,13] and consequently this value was adopted again here.

To compute the EFG tensor at iron, we utilized the Gaussian-98 program.[36] We used the "locally dense" basis set approach[39] used previously in which Fe has a Wachters' basis (62111111/3311111/3111),[40] all other heavy atoms have a 6-311G* basis, and hydrogen a 6-31G* basis. Both the pure functional BPW91 (Becke 88 exchange[41] and PW91[42] correlation functionals) and the hybrid functional B3LYP (Becke's three-parameter functional[43] with the LYP[44] correlation functional) were utilized, and calculations on the paramagnetic systems were of the spin-unrestricted type. A smaller set of calculations using B3PW91 (Becke's three-parameter functional[43] with the PW91[42] correlation functional), BHandHLYP (B stands for the Becke treatment[41]

(14) Debrunner, P. G. In *Iron Porphyrins*; Lever, A. B. P., Gray, H. B., Eds.; VCH Publishers: New York, 1989; Vol. 3, pp 139−234.
(15) Walker, F. A. *Coord. Chem. Rev.* **1999**, *185−186*, 471−534.
(16) Eicher, H.; Trautwein, A. *J. Chem. Phys.* **1969**, *50*, 2540. Eicher, H.; Trautwein, A. *J. Chem. Phys.* **1970**, *52*, 932. Huynh, B. H.; Papaefthymiou, G. C.; Yen, C. S.; Groves, J. L.; Wu, C. S. *J. Chem. Phys.* **1974**, *61*, 3750.
(17) Kent, T. A.; Spartalian, K.; Lang, G.; Yonetani, T.; Reed, C. A.; Collman, J. P. *Biochim. Biophys. Acta* **1979**, *580*, 245−258.
(18) Kent, T.; Spartalian, K.; Lang, G.; Yonetani, T. *Biochim. Biophys. Acta* **1977**, *490*, 331−340 and references therein.
(19) Oosterhuis, W. T.; Lang, G. *J. Chem. Phys.* **1969**, *50*, 4381−4387.
(20) Nasri, H.; Ellison, M. K.; Chen, S.; Huynh, B. H.; Scheidt, W. R. *J. Am. Chem. Soc.* **1997**, *119*, 6274−6283.
(21) Ellison, M. K.; Scheidt, W. R. *J. Am. Chem. Soc.* **1997**, *119*, 7404−7405.
(22) Bohle, D. S.; Debrunner, P.; Fitzgerald, J. P.; Hansert, B.; Hung, C.-H.; Thomson, A. J. *Chem. Commun.* **1997**, 91−92.
(23) Miller, L. M.; Pedraza, A. J.; Chance, M. R. *Biochemistry* **1997**, *36*, 12199−12207. Park, E. S.; Thomas, M. R.; Boxer, S. G. *J. Am. Chem. Soc.* **2000**, *122*, 12297−12303.
(24) Ellison, M. K.; Schultz, C. E.; Scheidt, W. R. *Inorg. Chem.* **1999**, *38*, 100−108. Ellison, M. K.; Schultz, C. E.; Scheidt, W. R. *Inorg. Chem.* **2000**, *39*, 5102−5110.
(25) Chien, J. C. W. *J. Chem. Phys.* **1969**, *51*, 4220−4227.
(26) Utterback, S. G.; Doetschman, D. C.; Szumowski, J.; Rizos, A. K. *J. Chem. Phys.* **1983**, *78*, 5874−5880.
(27) Hayes, R. G.; Ellison, M. K.; Scheidt, W. R. *Inorg. Chem.* **2000**, *39*, 3665−3668.
(28) Gochin, M.; Roder, H. *Protein Sci.* **1995**, *4*, 296−305.
(29) Yamamoto, Y. *Annu. Rep. NMR Spectrosc.* **1998**, *36*, 1−77.
(30) Shirazi, A.; Leum, E.; Goff, H. M. *Inorg. Chem.* **1983**, *22*, 360−362.
(31) Yamamoto, Y.; Chûjô, R. *J. Chem. Soc., Chem. Commun.* **1992**, 87−89.
(32) Goff, H. M. *J. Am. Chem. Soc.* **1981**, *103*, 3714−3722. Turner, P.; Gunter, M. J. *Inorg. Chem.* **1994**, *33*, 1406−1415.
(33) Obara, S.; Kashiwagi, H. *J. Chem. Phys.* **1982**, *77*, 3155−3165.
(34) Saito, M.; Kashiwagi, H. *Chem. Phys. Lett.* **1989**, *155*, 557−562.
(35) Karpov, A. A.; Khleskov, V. I.; Smirnov, A. B. *J. Struct. Chem.* **1993**, *34*, 731−734.
(36) Frisch, M. J.; Trucks, G. W.; Schlegel, H. B.; Scuseria, G. E.; Robb, M. A.; Cheeseman, J. R.; Zakrzewski, V. G.; Montgomery, J. A., Jr.; Stratmann, R. E.; Burant, J. C.; Dapprich, S.; Millam, J. M.; Daniels, A. D.; Kudin, K. N.; Strain, M. C.; Farkas, O.; Tomasi, J.; Barone, V.; Cossi, M.; Cammi, R.; Mennucci, B.; Pomelli, C.; Adamo, C.; Clifford, S.; Ochterski, J.; Petersson, G. A.; Ayala, P. Y.; Cui, Q.; Morokuma, K.; Malick, D. K.; Rabuck, A. D.; Raghavachari, K.; Foresman, J. B.; Cioslowski, J.; Ortiz, J. V.; Baboul, A. G.; Stefanov, B. B.; Liu, G.; Liashenko, A.; Piskorz, P.; Komaromi, I.; Gomperts, R.; Martin, R. L.; Fox, D. J.; Keith, T.; Al-Laham, M. A.; Peng, C. Y.; Nanayakkara, A.; Challacombe, M.; Gill, P. M. W.; Johnson, B.; Chen, W.; Wong, M. W.; Andres, J. L.; Gonzalez, C.; Head-Gordon, M.; Replogle, E. S.; Pople, J. A. Gaussian-98, Revision A.9; Gaussian, Inc.: Pittsburgh, PA, 1998.
(37) Su, Z.; Coppens, P. *Acta Crystallogr.* **1996**, *A52*, 748−756.
(38) Dufek, P.; Blaha, P.; Schwarz, K. *Phys. Rev. Lett.* **1995**, *75*, 3545−3548.
(39) Chestnut, D. B.; Moore, K. D. *J. Comput. Chem.* **1989**, *10*, 648−659.
(40) Wachters, A. J. H. *J. Chem. Phys.* **1970**, *52*, 1033−1036. Wachters, A. J. H. IBM Technological Report RJ584; 1969. Basis sets were obtained from the Extensible Computational Chemistry Environment Basis Set Database, Version 1.0, as developed and distributed by the Molecular Science Computing Facility, Environmental and Molecular Science Laboratory, which is part of the Pacific Northwest Laboratory, P.O. Box 999, Richland, WA 99352, and is funded by the U. S. Department of Energy. The Pacific Northwest Laboratory is a multiprogram laboratory operated by Battelle Memorial Institute for the U. S. Department of Energy under contract DE-AC06-76RLO 1830. Contact David Feller, Karen Schuchardt, or Don Jones for further information.
(41) Becke, A. D. *Phys. Rev. A* **1988**, *38*, 3098−3100.
(42) Perdew, J. P.; Burke, K.; Wang, Y. *Phys. Rev. B* **1996**, *54*, 16533−16539.
(43) Becke, A. D. *J. Chem. Phys.* **1993**, *98*, 5648−52.
(44) Lee, C.; Yang, W.; Parr, R. G. *Phys. Rev. B* **1988**, *37*, 785−789.

of the exchange functional, HandH means half Hartree−Fock exchange and half Slater exchange, the correlation part being the LYP functional[44]) and mPW1PW91 (Adamo and Barone's Becke-style one-parameter functional[45] using modified PW exchange and PW91 correlation[42]) functionals and 20 other basis set schemes, together with restricted open-shell (RO) calculations, were also investigated (data not shown), but the basis set scheme/functionals discussed above performed best; indeed, this scheme is essentially identical to that we used previously for ^{57}Fe NMR shift calculations [12] as well as $V_{ii}/\Delta E_Q$ calculations in diamagnetic systems.[13] The only difference between the current and previous basis sets used lies in the slightly enlarged and uniform basis for the ligand atoms, which we used to facilitate accurate spin density calculations. Calculations were carried out by using Silicon Graphics (Mountain View, CA) O-200, O-300, and O-2000 computers. Visualizations were made by using the Cerius^2 program.[46]

We investigated all five possible paramagnetic spin states: $S = {}^1/_2$, 1, $^3/_2$, 2, and $^5/_2$ (d^5, d^6), together with a reinvestigation of seven $S = 0$ (d^6, d^8) systems studied previously,[12,13] but using the computational methods described above. The molecules investigated are described below and were used to create the structures used for the DFT calculations. When protein structures were investigated, only the heme−imidazole moiety was considered. The following modifications were typically made: phenyl groups of TPP (TPP = 5,10,15,20-tetraphenylporphyrinato) and the mesityl groups of TMP (TMP = 5,10,15,20-tetramesitylporphyrinato) were replaced with hydrogen atoms, and counterions (BF_4^- and ClO_4^-) were not included in the calculations. In deoxymyoglobin, deoxyhemoglobin, and metmyoglobin, heme periphery substituents were replaced by hydrogen atoms, as described previously for other heme protein systems.[11,12] The axial histidine ligand was represented by 5-methylimidazole. The justification for these truncations is severalfold: first, DFT calculations on full proteins are still beyond current computational resources; second, in previous work on ^{57}Fe NMR shifts and Mössbauer quadrupole splittings on heme protein models, we found good accord with experimental results using this approach;[11,12] and third, it seems unlikely that the inclusion of protein atoms would affect the results, since, for example, experimental Mössbauer EFG data on hemoglobin and myoglobin from numerous different species show no changes with protein structure.[18] While peripheral substituents can affect heme structure, our approach is to use existing X-ray structures (of both heme models and of hemes in metalloproteins) which already include such effects, since, as shown by Rovira et al.,[47] the use of geometry optimization on isolated porphyrins may lead to electronic ground states different from those seen in proteins, which can be expected to complicate the prediction of experimental Mössbauer results. Thus, we focus here on predicting experimental spectroscopic results using experimental structures. The structures of the paramagnetic systems investigated were as follows:

***S* = $^1/_2$.** For ferric low-spin hemes,[15] we used systems which represented both the usual $(d_{xy})^2(d_{xz}d_{yz})^3$ state and the more unusual $(d_{xz}d_{yz})^4(d_{xy})^1$ configuration. In the former case, [Fe(TMP)(*N*-MeIm)$_2$]ClO_4 was selected (*N*-MeIm = *N*-methylimidazole) and both of the molecules in the unit cell[48] (**1**) and (**2**) were investigated. For the latter spin state, two complexes, [Fe(TPP)(*t*-BuNC)$_2$]ClO_4 (**3**) and [Fe(OEP)(*t*-BuNC)$_2$]ClO_4 (**4**),[49] were considered (OEP = 2,3,7,8,12,13,17,18-octaethylporphinato; *t*-BuNC = *tert*-butylisocyanide). Both **3** and **4** have strong π-acceptor ligands, and it has been shown that the porphyrinate ring is strongly ruffled [49] and that EPR, Mössbauer, IR and ^{1}H NMR results imply a $(d_{xy})^1$ ground state.[49] Calculations on two crystal structures of the ferrous $S = {}^1/_2$ system Fe(OEP)(NO)[21] (**5**) and (**6**) were also performed, as a prelude to heme−NO structure prediction.

***S* = 1.** For the ferrous intermediate spin complex, Fe(TPP) (**7**) was chosen.[50]

***S* = $^3/_2$.** For the intermediate spin ferric complex, we investigated the [Fe(OEP)(3-Cl-py)]ClO_4 (**8**) system (3-Cl-py = 3-chloropyridine).[51]

***S* = 2.** For $S = 2$ calculations, the truncated heme moieties from two recent deoxymyoglobin structures were selected (Brookhaven Protein Database; http://www.rcsb.org/pdb/; 1BZP,[6] **9** and 1A6N,[52] **10**). We also investigated the hemes from deoxyhemoglobin, with both α (**11**) and β (**12**) subunits being calculated using the PDB structure 1IBE.[53]

***S* = $^5/_2$.** For high-spin ferric systems, both the heme from the protein (metmyoglobin (**13**), 1BZ6[6]) and the model compounds (Fe(TPP)Cl (**14**),[54] Fe(TPP)Br (**15**),[55] and [Fe(TPP)(EtOH)$_2$]BF_4 (**16**)[56]) were used, representing both five- and six-coordinate geometries.

We also investigated the heme moieties in the $S = 0$ systems carbonmonoxymyoglobin, MbCO (**17**), Fe(TPP)(1-MeIm)(^{i}PrNC) (**18**), $Fe(CO)_5$ (**19**), $Fe(CO)_3$(1,4-butadiene) (**20**), Fe(CO)(propenal) (**21**), and $Fe(CO)_3$(cyclobutadiene) (**22**) investigated previously (but with different functionals/basis sets): structures are cited in refs 12 and 13, in addition to Fe(II)(TPP)(pyr)$_2$, (pyr = pyridine) (**23**).[57]

Results and Discussion

We show in Tables 1 and 2 the calculated ^{57}Fe Mössbauer electric field gradient tensor information computed by using the UBPW91 and UB3LYP functional approach and the locally dense basis set scheme described above, for 16 paramagnetic metalloporphyrins and model compounds. In addition, we also show results for six $S = 0$ systems investigated previously, but with the current functional/basis schemes (spin restricted calculations), together with results for Fe(II)(TPP)(pyr)$_2$. The excellent reproduction of all of the experimental quadrupole splitting results is clear from Tables 1 and 2 and is depicted graphically in Figures 1 and 2. For the BPW91 calculation, we find $R^2 = 0.975$, slope = 0.99, intercept = −0.08 mm sec^{-1}, and a root-mean-square deviation (rmsd) of 0.30 mm s^{-1} for 23 calculated molecules. For the B3LYP calculations, we find $R^2 = 0.978$, slope = 1.12, intercept = −0.26 mm sec^{-1}, and rmsd = 0.31 mm sec^{-1}. The addition of other diamagnetic data points from previous B3LYP calculations[13] into the current B3LYP data set has essentially no effect on the correlation: $R^2 = 0.976$, slope = 1.12, intercept = −0.21 mm sec^{-1}, and rmsd = 0.29 mm sec^{-1} ($N = 33$). We also show in Tables 1 and 2 values of ΔS_1 and ΔS_2, which are the deviations of the computed expectation values of the operator S^2 from ideal values, before and after annihilation, respectively. As indicated by the small ΔS_1 and the close-to-zero ΔS_2 values for both BPW91 and B3LYP results, these U-type calculations do not suffer from significant spin contamination, although, as expected, the effects are largest for the integral spin systems

(45) Adamo, C.; Barone, V. *J. Chem. Phys.* **1998**, *108*, 664−675.
(46) Cerius^2 Modelling Environment, Version 4.5; Molecular Simulation Inc., San Diego, CA, 2000.
(47) Rovira, C.; Kunc, K.; Hutter, J.; Ballone, P.; Parrinello, M. *J. Phys. Chem. A* **1997**, *101*, 8914−8925.
(48) Safo, M. K.; Gupta, G. P.; Walker, F. A.; Scheidt, W. R. *J. Am. Chem. Soc.* **1991**, *113*, 5497−5510. The ΔE_Q sign of [Fe(TMP)(*N*-MeIm)$_2$]ClO_4 was provided in a private communication from F. A. Walker.
(49) Walker, F. A.; Nasri, H.; Turowska-Tyrk, I.; Mohanrao, K.; Watson, C. T.; Shokhirev, N. V.; Debrunner, P. G.; Scheidt, W. R. *J. Am. Chem. Soc.* **1996**, *118*, 12109−12118.
(50) Collman, J. P.; Hoard, J. L.; Kim, N.; Lang, G.; Reed, C. A. *J. Am. Chem. Soc.* **1975**, *97*, 2676−2681.
(51) Scheidt, W. R.; Geiger, D. K.; Lee, Y. J.; Reed, C. A.; Lang, G. *Inorg. Chem.* **1987**, *26*, 1039−1045.
(52) Vojtechovsky, J.; Berendzen, J.; Chu, K.; Schlichting, I.; Sweet, R. M. *Biophys. J.* **1999**, *77*, 2153−2174.
(53) Wilson, J.; Phillips, K.; Luisi, B. *J. Mol. Biol.* **1996**, *264*, 743−756.
(54) Scheidt, W. R.; Finnegan, M. G. *Acta Crystallogr.* **1989**, C*45*, 1214−1216.
(55) Skelton, B. W.; White, A. H. *Aust. J. Chem.* **1977**, *30*, 2655−2660.
(56) Scheidt, W. R.; Geiger, D. K.; Lee, Y. J.; Gans, P.; Marchon, J.-C. *Inorg. Chem.* **1992**, *31*, 2660−2663.
(57) (a) Naiyin, L.; Coppens, P.; Landrum, J. *Inorg. Chem.* **1988**, *27*, 482−488. (b) Kobayashi, H.; Maeda, Y.; Yanagawa, Y. *Bull. Chem. Soc. Jpn.* **1970**, *43*, 2342−2346.

Table 1. Computational EFG and Related Electronic Properties from the BPW91 Calculations

	compound	S	ID[a]	R_1[b]	$^{expt}\Delta E_Q$[c] (mm s^{-1})	$^{exp}\eta$	T (K)	V_{xx} (au)	V_{yy} (au)	V_{zz} (au)	$\Delta E_Q{}^{calc}$ (mm s^{-1})	η^{calc}	$\rho_{\alpha\beta}{}^{Fe}$[d]	ΔS_1[e]	ΔS_2[e]
17	MbCO	0	1BZR	ref 6	+0.35[14]	<0.4	4.2	0.126	0.183	−0.308	0.50	0.18			
18	Fe(TPP)(1-MeIm)(^{i}PrNC)	0	FATYEE	0.0663[12]	+0.33[12]		77	0.188	0.203	−0.390	0.63	0.04			
19	$Fe(CO)_5$	0		ref 13	+2.51[13]	0.4	4.2	0.669	0.687	−1.356	2.20	0.01			
20	$Fe(CO)_3$(1,4-butadiene)	0		ref 13	−1.34[13]	0.4	4.2	−0.311	−0.526	0.837	−1.37	0.26			
21	Fe(CO)(propenal)	0		ref 13	+1.70[13]		4.2	0.068	0.962	−1.030	1.87	0.87			
22	$Fe(CO)_3$(cyclobutadiene)	0		ref 13	+1.52[13]		77	0.463	0.483	−0.946	1.53	0.02			
23	$Fe(TPP)(pyr)_2$	0	FUXTUN	ref 57a	+1.15[57b]		77	0.386	0.555	−0.941	1.53	0.18			
1	$[Fe(TMP)(N\text{-MeIm})_2]ClO_4$	$^1/_2$	$VOFMAE_1$	0.046[48]	−2.31[48]		4.2	−0.406	−1.180	1.586	−2.67	0.49	0.96	0.0145	0.0002
2			$VOFMAE_2$	0.046[48]	−2.31[48]		4.2	−0.341	−1.201	1.542	−2.62	0.56	0.96	0.0143	0.0002
3	$[Fe(TPP)(t\text{-BuNC})_2]ClO_4$	$^1/_2$	TUPXOR	0.104[49]	−1.89[49]	0.09	4.2	−0.626	−0.780	1.406	−2.28	0.11	0.77	0.0091	0.0001
4	$[Fe(OEP)(t\text{-BuNC})_2]ClO_4$	$^1/_2$	TUPXUX	0.052[49]	−1.80[49]	0.41	4.2	−0.324	−0.715	1.039	−1.72	0.38	0.69	0.0088	0.0001
5	Fe(OEP)(NO)	$^1/_2$	RIQSUF	0.0412[21]	+1.26[22]		100	0.351	0.459	−0.811	1.32	0.13	0.94	0.0197	0.0003
6	Fe(OEP)(NO)	$^1/_2$	RIQSUF01	0.0421[21]	+1.26[22]		100	0.347	0.469	−0.816	1.33	0.15	0.88	0.0012	0.0000
7	Fe(TPP)	1		0.074[50]	+1.51[50]		4.2	0.398	0.671	−1.068	1.75	0.26	2.16	0.0438	0.0008
8	$[Fe(OEP)(3\text{-Clpy})]ClO_4$	$^3/_2$	FEJCAY	0.093[51]	+3.23[14]		4.2	0.768	0.781	−1.548	2.51	0.01	2.60	0.0307	0.0003
9	deoxymyoglobin	2	1BZP	ref 6	−2.22[14]	0.7	4.2	−0.209	−1.147	1.355	−2.36	0.69	3.79	0.1264	0.0005
10			1A6N	ref 52	−2.22[14]	0.7	4.2	−0.503	−1.012	1.515	−2.50	0.34	3.80	0.1527	0.0007
11	deoxyhemoglobin	2	1IBE α	ref 53	−2.40[14]		4.2	−0.318	−0.939	1.257	−2.12	0.49	3.80	0.1831	0.0008
12		2	1IBE β	ref 53	−2.40[14]		4.2	−0.357	−1.018	1.375	−2.31	0.48	3.78	0.1262	0.0005
13	metmyoglobin	$^5/_2$	1BZ6	ref 6	+1.24[14]		4.2	0.324	0.427	−0.751	1.22	0.14	4.14	0.0068	0.0000
14	Fe(TPP)Cl	$^5/_2$	KANYUT	0.045[54]	+0.46[14]		4.2	0.017	0.104	−0.121	0.21	0.72	4.01	0.0069	0.0000
15	Fe(TPP)Br	$^5/_2$	BTPPFE	0.052[55]	+0.72[14]		4.2	0.044	0.108	−0.152	0.25	0.42	3.97	0.0078	0.0000
16	$[Fe(TPP)(EtOH)_2]BF_4$	$^5/_2$	TPFETB01	0.057[56]	+1.89[14]		4.2	0.347	0.523	−0.870	1.42	0.20	4.18	0.0061	0.0000

[a] The Protein Database or Cambridge Structure Database IDs are provided. [b] The structural references are listed as superscripts, and R_1 is the conventional residual factor of the crystal structures used. [c] The experimental references are superscripted below. [d] $\rho_{\alpha\beta}{}^{Fe}$ is the Mulliken spin density on the iron atom, in au. [e] ΔS_1 and ΔS_2 are the deviations of the computed expectation values of the operator S^2 from ideal values, before and after annihilation, respectively.

Table 2. Computational EFG and Related Electronic Properties from the B3LYP Calculations

	compound	S	ID[a]	R_1[b]	$^{expt}\Delta E_Q$[c] (mm s^{-1})	$^{exp}\eta$	T (K)	V_{xx} (au)	V_{yy} (au)	V_{zz} (au)	$\Delta E_Q{}^{calc}$ (mm s^{-1})	η^{calc}	$\rho_{\alpha\beta}{}^{Fe}$[d]	ΔS_1[e]	ΔS_2[e]
17	MbCO	0	1BZR	ref 6	+0.35[14]	<0.4	4.2	0.041	0.102	−0.143	0.27	0.42			
18	Fe(TPP)(1-MeIm)(^{i}PrNC)	0	FATYEE	0.0663[12]	+0.33[12]		77	0.083	0.096	−0.180	0.29	0.07			
19	$Fe(CO)_5$	0		ref 13	+2.51[13]	0.4	4.2	0.772	0.796	−1.568	2.54	0.02			
20	$Fe(CO)_3$(1,4-butadiene)	0		ref 13	−1.34[13]	0.4	4.2	−0.388	−0.529	0.918	−1.49	0.15			
21	Fe(CO)(propenal)	0		ref 3	+1.70[13]		4.2	0.059	1.079	−1.138	2.08	0.90			
22	$Fe(CO)_3$(cyclobutadiene)	0		ref 13	+1.52[13]		77	0.496	0.515	−1.011	1.64	0.02			
23	$Fe(TPP)(pyr)_2$	0	FUXTUN	ref 57a	+1.15[57b]		77	0.306	0.382	−0.688	1.12	0.11			
1	$[Fe(TMP)(N\text{-MeIm})_2]ClO_4$	$^1/_2$	$VOFMAE_1$	0.046[48]	−2.31[48]		4.2	−0.510	−1.154	1.664	−2.76	0.39	1.02	0.0157	0.0002
2			$VOFMAE_2$	0.046[48]	−2.31[48]		4.2	−0.476	−1.184	1.660	−2.77	0.43	1.02	0.0150	0.0002
3	$[Fe(TPP)(t\text{-BuNC})_2]ClO_4$	$^1/_2$	TUPXOR	0.104[49]	−1.89[49]	0.09	4.2	−0.939	−1.110	2.049	−3.32	0.08	1.01	0.0109	0.0001
4	$[Fe(OEP)(t\text{-BuNC})_2]ClO_4$	$^1/_2$	TUPXUX	0.052[49]	−1.80[49]	0.41	4.2	−0.375	−1.104	1.478	−2.49	0.49	1.01	0.0155	0.0002
5	Fe(OEP)(NO)	$^1/_2$	RIQSUF	0.0412[21]	+1.26[22]		100	0.353	0.392	−0.745	1.21	0.05	1.12	0.1091	0.0029
6	Fe(OEP)(NO)	$^1/_2$	RIQSUF01	0.0421[21]	+1.26[22]		100	0.339	0.427	−0.766	1.24	0.12	1.15	0.1005	0.0026
7	Fe(TPP)	1		0.074[50]	+1.51[50]		4.2	0.209	0.538	−0.748	1.25	0.44	2.12	0.0296	0.0004
8	$[Fe(OEP)(3\text{-Clpy})]ClO_4$	$^3/_2$	FEJCAY	0.093[51]	+3.23[14]		4.2	0.837	0.884	−1.721	2.79	0.03	2.76	0.0396	0.0004
9	deoxymyoglobin	2	1BZP	ref 6	−2.22[14]	0.7	4.2	−0.071	−1.483	1.554	−2.84	0.91	3.80	0.0637	0.0027
10			1A6N	ref 52	−2.22[14]	0.7	4.2	−0.080	−1.542	1.621	−2.96	0.90	3.79	0.0619	0.0002
11	deoxyhemoglobin	2	1IBE α	ref 53	−2.40[14]		4.2	−0.195	−1.274	1.469	−2.59	0.73	3.80	0.1019	0.0004
12		2	1IBE β	ref 53	−2.40[14]		4.2	−0.316	−1.262	1.578	−2.71	0.60	3.80	0.0762	0.0003
13	metmyoglobin	$^5/_2$	1BZ6	ref 6	+1.24[14]		4.2	0.408	0.484	−0.892	1.45	0.09	4.28	0.0080	0.0000
14	Fe(TPP)Cl	$^5/_2$	KANYUT	0.045[54]	+0.46[14]		4.2	0.048	0.149	−0.197	0.33	0.52	4.11	0.0110	0.0000
15	Fe(TPP)Br	$^5/_2$	BTPPFE	0.052[55]	+0.72[14]		4.2	0.072	0.147	−0.218	0.36	0.34	4.07	0.0125	0.0000
16	$[Fe(TPP)(EtOH)_2]BF_4$	$^5/_2$	TPFETB01	0.057[56]	+1.89[14]		4.2	0.431	0.620	−1.050	1.71	0.18	4.29	0.0074	0.0000

[a] The Protein Database or Cambridge Structure Database IDs are provided. [b] The structural references are listed as superscripts, and R_1 is the conventional residual factor of the crystal structures used. [c] The experimental references are superscripted below. [d] $\rho_{\alpha\beta}{}^{Fe}$ is the Mulliken spin density on the iron atom, in au. [e] ΔS_1 and ΔS_2 are the deviations of the computed expectation values of the operator S^2 from ideal values, before and after annihilation, respectively.

(∼2−3%, before annihilation). When considering the large range of the experimental data, 5.63 mm s^{-1}, the wide range of spin states, and the fact that there was no geometry optimization or structural refinement on any of the crystal structures used, these results show that it is now possible to quite accurately predict Mössbauer ΔE_Q values in paramagnetic as well as the diamagnetic heme systems and related molecules.[12,58]

As shown in Figure 3 for the heme model complexes, larger deviations between theory and experiment appear to occur for those systems with poorer crystal structures, that is, those with the larger R_1 values in Tables 1 and 2 ($R = 0.667$, $p < 0.05$, $N = 12$ and $R = 0.916$, $p < 0.0001$, $N = 12$, respectively, for the BPW91 and B3LYP predicted values from the theory versus experiment correlations). It may thus be possible to improve the quality of the predictions even further, by geometry optimization. However, it is also clear that the rms error of ∼0.30 mm sec^{-1} over the 5.63 mm sec^{-1} range in ΔE_Q is

(58) Grodzicki, M.; Flint, H.; Winkler, H.; Walker, F. A.; Trautwein, A. X. *J. Phys. Chem.* **1997**, *101*, 4202−4207. Zakharieva, O.; Schünemann, V.; Gerdan, M.; Licoccia, S.; Cai, S.; Walker, F. A.; Trautwein, A. X. *J. Am. Chem. Soc.* **2002**, *124*, 6636−6648.

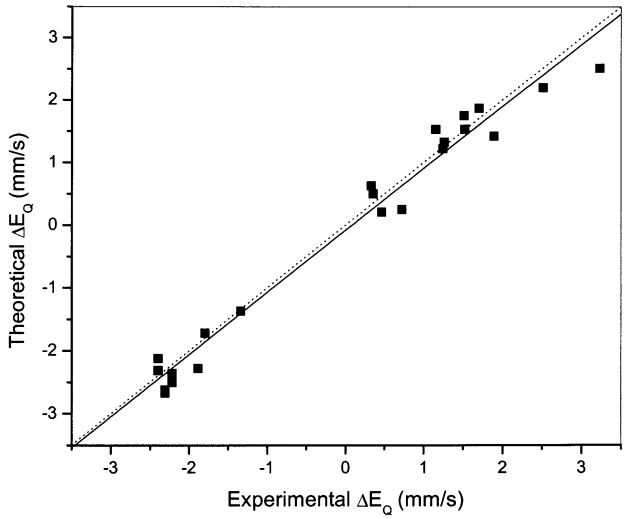

Figure 1. Relationship between the theoretical and experimental ^{57}Fe Mössbauer quadrupole splitting parameters (BPW91 functional calculations). The dotted line represents the ideal 1:1 correlation or "45° slope" line.

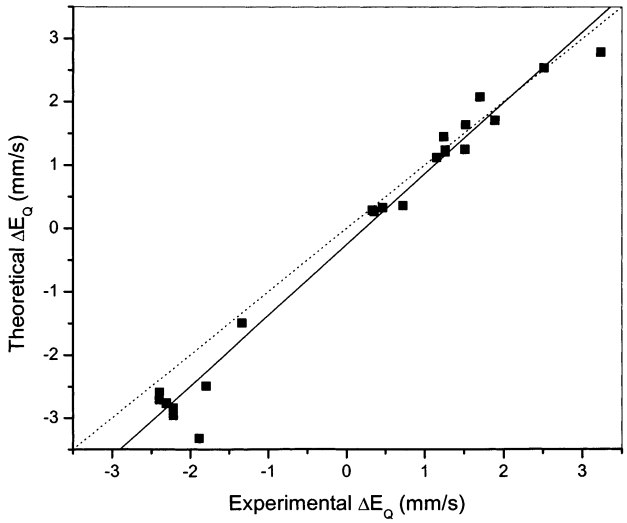

Figure 2. Relationship between the theoretical and experimental ^{57}Fe Mössbauer quadrupole splitting parameters (B3LYP functional calculations). The dotted line represents the ideal 1:1 correlation or "45° slope" line.

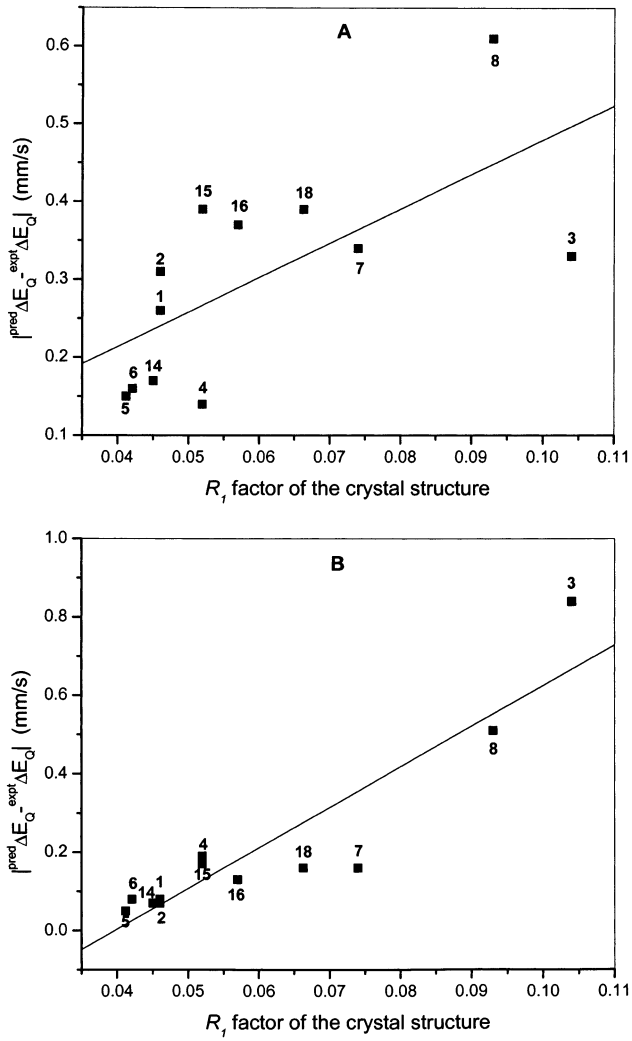

Figure 3. Graphs showing differences between predicted (from theory versus experiment correlations) and experimental quadrupole splitting parameters as a function of crystallographic R_1 factors for the heme model systems investigated. (A) BPW91, $|^{\text{pred}}\Delta E_Q - {}^{\text{expt}}\Delta E_Q| = 0.04 + 4.42\ R_1$; $R = 0.667$, $p < 0.05$, $N = 12$; (B) B3LYP, $|^{\text{pred}}\Delta E_Q - {}^{\text{expt}}\Delta E_Q| = -0.41 + 10.35\ R_1$; $R = 0.916$, $p < 0.0001$, $N = 12$.

already very small. It is also interesting to note that although in Figures 1 and 2 the intermediate spin species exhibit larger deviations than do the more conventional spin states, they are still close enough to the correlation line that they do not degrade the overall correlation significantly. For example, without the $S = {}^3/_2$ Fe(III) and $S = 1$ Fe(II) points, we find $R^2 = 0.979$, slope = 1.01, intercept = -0.07 mm s^{-1}, and rmsd = 0.27 mm s^{-1} when using the BPW91 functional and $R^2 = 0.981$, slope = 1.16, intercept = -0.21mm s^{-1}, and rmsd = 0.29 mm s^{-1} with B3LYP. This shows that the final computational model behaves well for all six different spin states investigated, covering 23 different molecules. The overall agreement between theory and experiment is comparable to the results reported previously on solely diamagnetic systems,[13] $R^2 = 0.975$, slope = 1.04, rmsd = 0.18 mm sec^{-1} ($N = 14$ and a range of 3.93 mm sec^{-1}), the rmsd being about 5% of the overall range for both diamagnetic and paramagnetic systems.

In addition to predicting ΔE_Q, the asymmetry parameters, η, of the electric field gradient tensor in the paramagnetic systems are also well reproduced. For high-spin ferrous deoxymyoglobin ($S = 2$), we obtain $\eta = 0.69$ for the BPW91 calculation and $\eta = 0.91$ for the B3LYP result, essentially the same as the $\eta = 0.7$ result obtained experimentally.[14] The computed η value for the unusual ferric low-spin $(d_{xz},d_{yz})^4(d_{xy})^1$ complex [Fe(TPP)(*t*-BuNC)$_2$]ClO$_4$ is 0.11 (BPW91) or 0.08 (B3LYP), which is also very close to the experimental value of 0.09.[49] The experimental η 0.41 measured at 150 K for another ferric low-spin $(d_{xz},d_{yz})^4(d_{xy})^1$ complex [Fe(OEP)(*t*-BuNC)$_2$]ClO$_4$[49] is also close to our computed values of 0.38 (BPW91) or 0.49 (B3LYP). However, since η values are rather difficult to measure experimentally, we believe that more confidence in the predictive ability of the calculations can arguably be placed in the ΔE_Q predictions.

In addition to computing all nine components of the electric field gradient tensor, the DFT calculations provide information on the orientations of these components in a molecular axis system. The orientations of the principal components of the computed EFG tensors, V_{xx}, V_{yy}, and V_{zz}, are illustrated graphically in Figure 4 for some of the

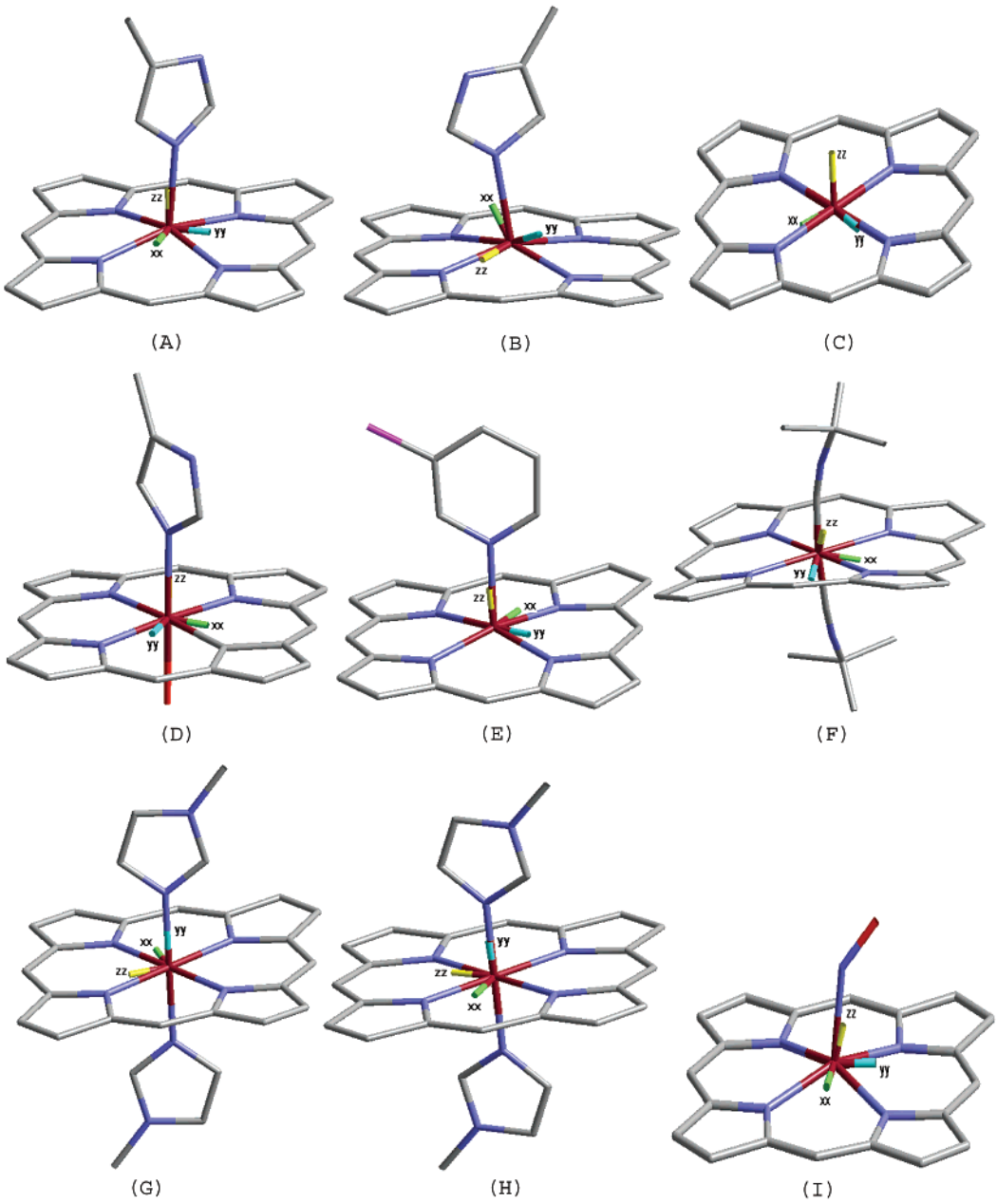

Figure 4. Selected EFG tensor orientations for calculated paramagnetic systems. All hydrogen atoms and porphyrin peripheral substituents have been eliminated for clarity. (A) deoxymyoglobin ($S = 2$); (B) deoxyhemoglobin-β ($S = 2$); (C) Fe(TPP) ($S = 1$); (D) metmyoglobin ($S = {}^5/_2$); (E) [Fe(OEP)-(3-Clpy)]ClO_4 ($S = {}^3/_2$); (F) [Fe(OEP)(*t*-BuNC)$_2$]ClO_4 ($S = {}^1/_2$); (G) [Fe(TMP)(*N*-MeIm)$_2$]ClO_4 (molecule 1) ($S = {}^1/_2$); (H) [Fe(TMP)(*N*-MeIm)$_2$]ClO_4 (molecule 2) ($S = {}^1/_2$); (I) Fe(OEP)(NO), RIQSUF ($S = {}^1/_2$).

paramagnetic molecules investigated. Experimental studies on high spin ferrous ($S = 2$) heme proteins[18,59] indicate a low symmetry of the electron wave function, which bears no relation to the essentially 4-fold symmetry of the porphyrin.[14] This can also be seen from the orientation of the computed EFG tensor principal axes in deoxymyoglobin (Figure 4A) and particularly in deoxyhemoglobin (Figure 4B). This effect may come from the presence of the axial imidazole ligand to the porphyrin in these deoxy-heme proteins. A recent DFT study[47] has already shown the important effect on the energy gaps among frontier molecular orbitals by the imidazole ligand and demonstrated its clear effect in controlling the electronic structure of the iron porphyrin by small structural distortions in the Fe-imidazole geometry, and there are large variations in the Fe-imidazole geometry in the X-ray structures of deoxy-heme proteins. For example, the distance between iron and its coordinated nitrogen in the imidazole ligand differs by as much as 0.14 Å in deoxymyoglobins[6] and the deoxyhemoglobin β subunit.[53] The Mössbauer experiment[18] suggested two possible EFG tensor orientations, and the porphyrin normal was not coincident with V_{zz} in either of them. One Mössbauer result was similar to our deoxymyoglobin results, while the other was similar to that we find in deoxyhemoglobin. In contrast, the EFG tensor orientations coincide well with porphyrin symmetry for the ferrous $S = 1$ system (Figure 4C). Experimental studies on ferric high-spin ($S = {}^5/_2$) systems have included both model

(59) Champion, P. M.; Lipscomb, J. D.; Münck, E.; Debrunner, P. G.; Gunsalus, I. C. *Biochemistry* **1975**, *14*, 4151−4158.

compounds[14] and metmyoglobin[60] and showed that V_{zz} is along the heme normal. This is also what we find in the DFT calculations, as demonstrated by the metmyoglobin result, illustrated in Figure 4D. Such a result was also found theoretically for the ferric intermediate spin complex illustrated in Figure 4E as well as in some related experimental studies.[14] Figure 4F shows, in the unusual ferric low-spin $(d_{xz},d_{yz})^4(d_{xy})^1$ complexes, as exemplified by $[Fe(OEP)(t\text{-BuNC})_2]ClO_4$, that although the large porphyrin ruffling distorts V_{xx} and V_{yy} away from the porphyrin symmetry axes, V_{zz} is still essentially along the heme normal, as found experimentally.[49] However, in two other low-spin ferric ($S = {}^1/_2$) molecules (having the same molecular formula, $[Fe(TMP)(N\text{-MeIm})_2]ClO_4$), V_{zz} is essentially in the heme plane. But the EFG tensor orientations of these two $[Fe(TMP)(N\text{-MeIm})_2]^+$ molecules differ somewhat, because of slightly different orientations of the axial ligand,[48] *N*-methylimidazole (Figure 4G and H). In the ferrous $S = {}^1/_2$ NO complexes, V_{xx} and V_{yy} are along the meso-diagonal lines of the porphyrin, while V_{zz} is close to the heme normal (Figure 4I).

The experimental Mössbauer spectroscopic studies only reported single ΔE_Q values for $[Fe(TMP)(N\text{-MeIm})_2]ClO_4$ and deoxyhemoglobin, while each species has two molecules or subunits in the unit cell. Our calculations predict slightly different EFG tensors and tensor orientations for each of the structurally different pairs of molecules or subunits. In the case of $[Fe(TMP)(N\text{-MeIm})_2]ClO_4$, the EFG predictions differ by only 0.05 mm s^{-1}, which is too small to be detected experimentally, but examination of the crystal structure suggests that this ΔE_Q difference may be associated with a 0.01 Å variation in the axial ligand−iron distance. This kind of structural sensitivity would be similar to that found in distance-dependent ΔE_Q calculations on $Fe(P)(pyr)_2$ models, where ΔE_Q decreases by 0.5 mm s^{-1} when the $Fe-N_{pyr}$ bond length is reduced by 0.1 Å.[34] In contrast to these model compound studies, any analysis of structural effects on the EFG in the deoxyhemoglobin subunits will be more complicated because of the larger uncertainties in the X-ray structure of this large protein. For example, the distance between iron and its coordinated nitrogen in the imidazole ligand differs as much as 0.09 Å in α and β subunits. In the case of Fe(OEP)NO, the two crystal structures investigated are very similar, as reflected in the close agreement in computed ΔE_Q values using either the BPW91 or B3LYP functionals.

The results we have described above give some confidence in the "quality" of the calculations in the sense that it is now clearly possible to compute ^{57}Fe Mössbauer ΔE_Q values with about a 0.3 mm sec^{-1} rmsd over a 5.63 mm sec^{-1} range in ΔE_Q values with a slope very close to 1 and $p < 0.0001$, in addition to being able to reproduce the available η and EFG tensor orientation results. In addition, as we shall describe elsewhere,[61] the ^{1}H, ^{13}C, ^{15}N, and ^{19}F NMR hyperfine shifts can also be quite successfully predicted over an ~6000 ppm shift range using the calculational schemes described above, in paramagnetic metalloporphyrin/metalloprotein systems, as can isotropic hyperfine tensors in ESR spectra.[62] This gives some confidence in the use of this approach to investigate electronic structure per se, and consequently, we give here a brief discussion of the electronic structures of several of the more interesting systems investigated in this work.

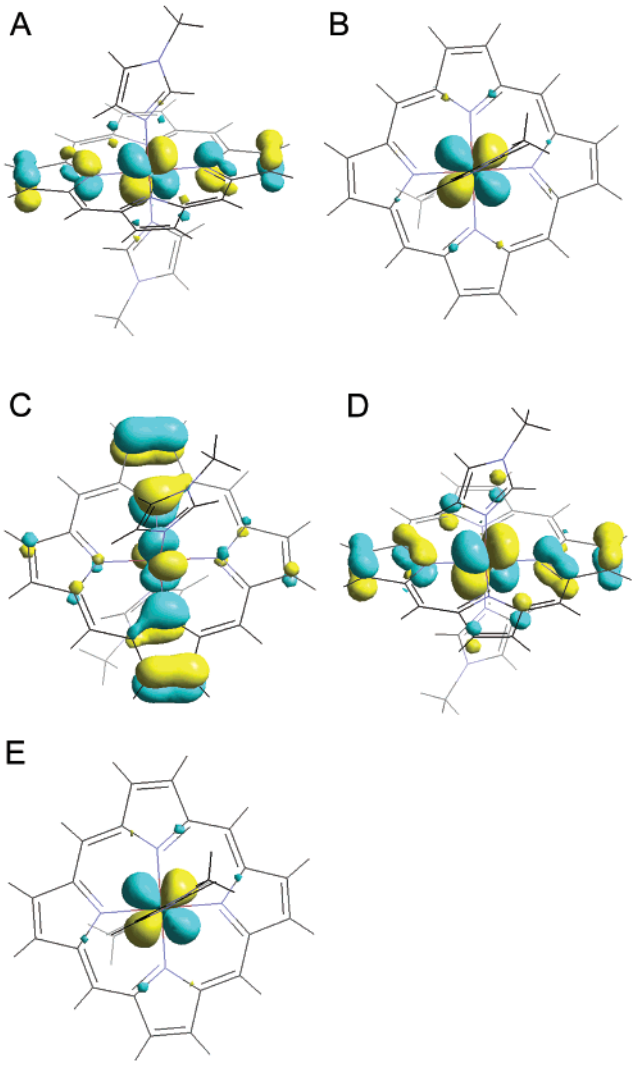

Figure 5. Isosurface representation of the frontier molecular orbitals for the $[Fe(TMP)(1\text{-MeIm})_2]^+$ model system: (A) αHOMO-1; (B) αHOMO-3; (C) αHOMO-4; (D) βHOMO; (E) βHOMO-1 (contour values = ±0.04, 0.04, 0.04, 0.08, and 0.04 au, respectively).

For paramagnetic systems, both α- and β-spin electrons need to be considered and it is often not a simple matter to map the individual α,β MOs to a conventional ligand field picture. Nevertheless, there is considerable interest in the structures of $S = {}^1/_2$ ferric proteins and model systems, as well as NO−heme adducts, where there are important questions related to charge and spin density distributions: what, for example, is the charge on iron in the NO species? We, therefore, first investigate the topic of the electronic structure and spin density distribution in the Fe(III) $S = {}^1/_2$ systems $[Fe(TMP)(1\text{-MeIm})_2]^+$ and $[Fe(OEP)(t\text{-BuNC})_2]^+$. The former compound has a highly planar porphyrin and a "conventional" $(d_{xy})^2(d_{xy},d_{yz})^3$ configuration in which d_{xy}, which is in the plane of the porphyrin, is filled and the unpaired electron resides in either d_{xz} or d_{yz}.[48] On the other hand, $[Fe(OEP)(t\text{-BuNC})]_2^+$ has a very highly distorted porphyrin, because of the strong π-acceptor *t*-BuNC ligands, and it is thought that the iron configuration is $(d_{xz},d_{yz})^4(d_{xy})^1$ in which the unpaired electron

(60) Harami, T. *J. Chem. Phys.* **1979**, *71*, 1309−1318.
(61) Mao, J.; Zhang, Y.; Oldfield, E. *J. Am. Chem. Soc.* **2002**, *124*, 13911−13920.
(62) Gossman, B.; Zhang, Y.; Oldfield, E., unpublished results.

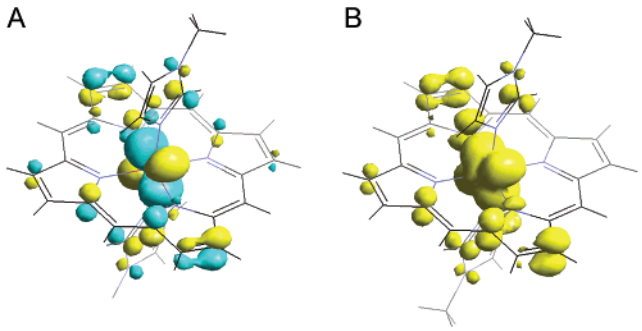

Figure 6. (A) βLUMO and (B) total spin density of $[Fe(TMP)(1\text{-}MeIm)_2]^+$ model system (contour values = ±0.09 and 0.001 au, respectively).

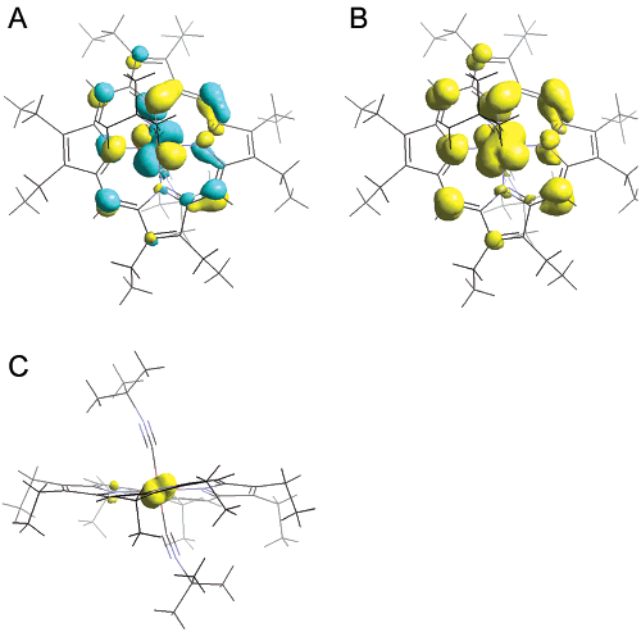

Figure 7. (A) βLUMO, (B) total spin density (top view), and (C) total spin density (side view) for the $[Fe(OEP)(t\text{-}BuNC)_2]^+$ model system (contour values = ±0.09, 0.001, and 0.01 au, respectively).

is primarily in d_{xy}, in the porphyrin plane, together with substantial delocalization to the heme meso-positions.[49]

We show in Figure 5 a selection of occupied α- and β-MOs for the $[Fe(TMP)(1\text{-}MeIm)_2]^+$ model, from which it can be seen (Figure 5A−C) that the α-spin d_{xz}, d_{xy}, and d_{yz} orbitals are occupied, while for the β spins (Figures 5D and E), we find that d_{yz} and d_{xy} are occupied. This corresponds to $(d_{xy})^2(d_{xz},d_{yz})^3$, clearly the same picture as the conventional ligand field description for the metal. The spin-density distribution in $S = {}^1/_2$ systems is known to map onto the β-LUMO,[63] with a general similarity in topological distribution, though they are different in signs, phases, or nodal planes. The β-LUMO (isosurface at ±0.09 au) in the $[Fe(TMP)(1\text{-}MeIm)_2]^+$ model, Figure 6A, together with the total spin density isosurface (at 0.001 au), Figure 6B, clearly indicate that most of the spin density is localized in a d_{xz}/d_{yz} metal orbital. In sharp contrast, however, for the $[Fe(OEP)(t\text{-}BuNC)_2]^+$ model, we find that the unpaired electron is localized in the d_{xy} orbital, Figure 7A and B, in the plane of the porphyrin, which as can be seen in the side view in Figure 7C, is highly ruffled. As described elsewhere,[49] this

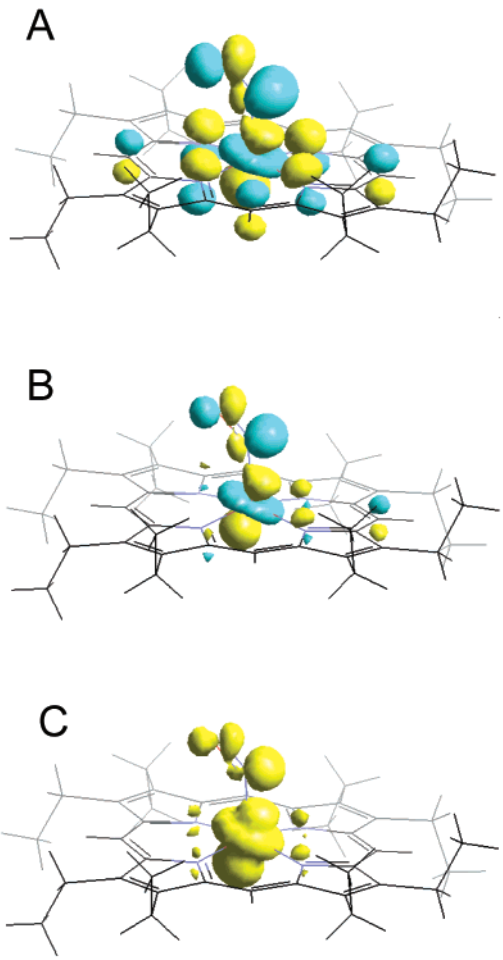

Figure 8. (A) αHOMO, (B) βLUMO, and (C) total spin density of the Fe(OEP)(NO) model system (contour values = ±0.1, ±0.06, and 0.003 au, respectively).

ruffling permits overlap between the porphyrin $3a_{2u}(\pi)$ orbital and the Fe d_{xy} orbital, together with considerable spin density delocalization onto the porphyrin carbon/hydrogen atoms, and there is clearly a large spin density visible on the meso-carbons in Figure 7B, which explains a large upfield meso-H NMR hyperfine shift seen experimentally.[49]

Next, we consider the case of Fe(OEP)(NO), where the valence on Fe is of interest. Here, the Mössbauer ΔE_Q is again predicted with good accuracy in the calculations (experiment, 1.26 mm sec^{-1}; calculated, 1.32 and 1.33 mm sec^{-1}), which gives some confidence in the calculations. As shown in Figure 8A, the HOMO for the OEP model is primarily of Fe d_z^2 character, in general accord with the results of previous calculations,[47,64−66] and as expected, the β-LUMO (Figure 8B) reflects the total spin density distribution (Figure 8C), with most of the spin density localized on Fe. In this case, the Mulliken spin density on Fe is 0.94 (0.88) *e* (two different crystal structures were investigated for this molecule using the BPW91 functional). This result is consistent with other recent DFT calculations on ferrous NO porphyrins.[47,64,66] In contrast, the NO moiety in this molecule has only a residual spin density, as pointed out in another recent DFT study.[47] Both sets of

(63) George, S. D.; Metz, M.; Szilagyi, R. K.; Wang, H.; Cramer, S. P.; Lu, Y.; Tolman, W. B.; Hedman, B.; Hodgson, K. O.; Solomon, E. I. *J. Am. Chem. Soc.* **2001**, *123*, 5757−5767.
(64) Hayes, P. G.; Ellison, M. K.; Scheidt, W. R. *Inorg. Chem.* **2000**, *39*, 3665−3668.
(65) Ghosh, A.; Wondimagegn, T. *J. Am. Chem. Soc.* **2000**, *122*, 8101−8102.
(66) Patchkovskii, S.; Ziegler, T. *Inorg. Chem.* **2000**, *39*, 5354−5364.

calculations favor an almost sinusoidal spin density for the NO moiety, with both N and O atoms having spin densities opposite to that of Fe, and a compensating spin density in the middle of the NO bond.[47] This supports the picture of an almost neutral NO (Mulliken formal charge ~ -0.1 *e*) with a very small net spin density (Mulliken spin densities < 0.1 *e*). Similarly, the experimental N−O bond lengths are both ~1.17 Å,[21] which are rather close to free NO (1.15 Å, to be compared with 1.06 Å for NO^+ and 1.26 Å for NO^-).[67,68] Also, the experimental N−O bond stretching frequency (~1670 cm^{-1})[21,22] is closer to a neutral NO value (1876 cm^{-1}, versus 2345 cm^{-1} for NO^+ and 1284 cm^{-1} for NO^-).[67,68]

To help ensure these results were not dependent on the calculational methods used, we also performed a relativistic DFT calculation (using the zero-order regular approximation, ZORA, method) on one Fe(OEP)NO crystal structure (**6**) using the BPW91 functional with an uncontracted triple-ζ all electron STO basis set (ZORA-V) with the Amsterdam Density Functional (ADF) program.[69,70] The computed Mössbauer quadrupole splitting and asymmetry parameter (1.34 mm s^{-1}; 0.15) were very close to the Gaussian-98 results (1.33 mm s^{-1}; 0.13) shown in Table 1. The Mulliken spin density analysis using ADF also showed good agreement with the Gaussian-98 values. In addition, a population analyses based on the Mulliken, Hirshfeld, and Voronoi deformation density methods (in ADF)[70] also support the picture of an approximately neutral NO fragment (formal charge < -0.1 *e*) in this complex. And, finally, an NBO population analysis[71] on the Gaussian-98 results revealed that iron has approximately 7 d electrons in both BPW91 and B3LYP calculations, as also found in the ADF Mulliken population analysis. A simple classification of this NO complex as (d^5)Fe(III) ($S = {}^1/_2$) NO^- ($S = 0$), (d^6)Fe(II) ($S = 0$) NO ($S = {}^1/_2$), or (d^7)Fe(I) ($S = {}^1/_2$) NO^+ ($S = 0$) seems not to be feasible, on the basis of inspection of the molecular orbitals, spin, and charge density results,[47] although both the ^{57}Fe Mössbauer quadrupole splitting and the ^{14}N hyperfine coupling constant[62] can be accurately predicted from the computed wave functions.

Finally, we expand our discussion on the intermediate spin system Fe(TPP) ($S = 1$), since there exists a wealth of contradicting experimental and theoretical investigations.[33,72−78] For example, NMR,[72] X-ray,[73−74] and magnetic susceptibility[75] measurements suggest a $^3A_{2g}$ ground state. An early SW-Xα calculation[76] also predicted the same ground state, and a Hartree−Fock calculation[33] showed that $^3A_{2g}$ is the lowest triplet state but with a high-spin ground state. On the other hand, a ^3E_g ground state was inferred from the resonance Raman spectra,[77] which was also predicted by a more recent LDA calculation.[78] In all these investigations, a D_{4h} geometry was assumed. However, with this imposed D_{4h} structure, our DFT calculation yielded a large and negative quadrupole splitting of -3.72 mm s^{-1} (BPW91), in poor accord with the experimental value of $+1.51$ mm s^{-1}.[50] In this situation, however, the final charge densities automatically break down the D_{4h} symmetry, which suggests that a lower symmetry due to Jahn−Teller distortion might be operating. This phenomenon was also mentioned in a recent DFT geometry optimization on Fe(P) without symmetry constraints.[47] In fact, the D_{2d} crystal structure[50] has only a very small difference from the D_{4h} structure, as evidenced by the 0.01 Å structural differences between neighboring $N-C_\alpha$ and $C_\alpha-C_\beta$ bond lengths. The electronic energy of the D_{2d} molecule is somewhat lower than that of the corresponding D_{4h} configuration, as expected from a Jahn−Teller distortion, but the relative ordering of the spin densities of the α, β, and meso-carbons are the same in both structures. However, the computed ΔE_Q for the D_{2d} structure is 1.75 mm s^{-1} (BPW91), which is now much closer to the experimental value of 1.51 mm s^{-1}.[50] Our B3LYP result for this intermediate spin system has a similar deviation from the experimental value. The low-lying excited states[78] in this molecule make it difficult to generate a better result and may be responsible for the difference between these two functionals. In our calculations on Fe(TPP), all bond lengths and bond angles were taken from the crystal D_{2d} structure,[50] but planarity of the molecule, as suggested by DFT optimizations on Fe(P),[47] was also incorporated into the structure. So, the final symmetry-breaking charge densities of the D_{4h} molecule result in a C_{4h} configuration. The computed EFG data strongly suggest, therefore, that it is the structural variations of the porphyrin bond lengths and bond angles, rather than planarity, that are responsible for the incorrect EFG sign. Calculations on the Fe(TPP) unit from other crystal structures of Fe(TPP)L and Fe(TPP)L′ (L and L′ are axial ligands)[79] also yield the correct EFG sign, but the absolute values (0.62 and 0.54 mm s^{-1}) deviate considerably from experimental values. It should be noted that the structural differences are primarily in the Fe−N bond lengths, which are 1.991, 1.996, and 1.972 Å for Fe(TPP)L, Fe(TPP)L′, and Fe(TPP), respectively. These Fe−N bond lengths show an excellent correlation with the computed EFG data ($R^2 = 0.984$). The shorter Fe−N bond lengths increase electron density along the *xy* direction, which is expected to result in a larger ΔE_Q, as is found. These results indicate, therefore, that EFG results are extremely sensitive to structural changes around the iron atom, which could potentially be of use in future structural refinements.

Conclusions

The results we have discussed above are of interest for a number of reasons. First, we have used DFT methods to compute the Mössbauer quadrupole splittings for a wide range of

(67) Cotton, F. A.; Wilkinson, G. *Advanced Inorganic Chemistry*, 4th ed.; John Wiley and Sons: New York, 1980.
(68) Laane, J.; Ohlsen, J. R. *Prog. Inorg. Chem.* **1980**, *27*, 465−513. Kim, E. K.; Kochi, J. K. *J. Am. Chem. Soc.* **1991**, *113*, 4962−4974. Maricq, M. M.; Tanguay, N. A.; O'Brien, J. C.; Rodday, S. M.; Rinden, E. *J. Chem. Phys.* **1989**, *90*, 3136−3144.
(69) ADF 2000.02. http://www.scm.com, Vrije Universiteit, Theoretical Chemistry, Amsterdam, The Netherlands.
(70) Te Velde, G.; Bickelhaupt, F. M.; Baerends, E. J.; Fonseca Guerra, C.; Van Gisbergen, S. J. A.; Snijders, J. G.; Ziegler, T. *J. Comput. Chem.* **2001**, *22*, 931−967 and references therein.
(71) Glendening, E. D.; Reed, A. E.; Carpenter, J. E.; Weinhold, F. NBO Version 3.1; Theoretical Chemistry Institute, University of Wisconsin, Madison, WI.
(72) Goff, H.; LaMar, G. N.; Reed, C. A. *J. Am. Chem. Soc.* **1977**, *99*, 3641−3646.
(73) Li, N.; Su, Z.; Coppens, P.; Landrum, J. *J. Am. Chem. Soc.* **1990**, *112*, 7294−7298.
(74) Coppens, P. *J. Phys. Chem.* **1989**, *93*, 7979−7984.
(75) Boyd, P. D. W.; Buckingham, D. A.; McMeeking, R. F.; Mitra, S. *Inorg. Chem.* **1979**, *18*, 3585−3591.
(76) Sontum, S. F.; Case, D. A.; Karplus, M. *J. Chem. Phys.* **1983**, *79*, 2881−2892.
(77) Kitagama, T.; Teraoka, J. *Chem. Phys. Lett.* **1979**, *63*, 443−446.
(78) Delley, B. *Physica B* **1991**, *172*, 185−193.
(79) Byrn, M. P.; Curtis, C. J.; Goldberg, I.; Hsiou, Y.; Khan, S. I.; Sawin, P. A.; Tendick, S. K.; Strouse, C. E. *J. Am. Chem. Soc.* **1991**, *113*, 6549−6557.

paramagnetic heme proteins and model compounds having spin states $S = {}^1/_2$, 1, ${}^3/_2$, 2, and ${}^5/_2$. The calculational schemes employed also permit evaluation of $S = 0$ heme protein and model compound results. We find good agreement between experimental and computed ΔE_Q values ($R^2 = 0.975-0.978$, slope $= 0.99-1.12$, intercept $= -0.08$ to -0.26 mm s^{-1}, and rmsd $= 0.30-0.31$ mm s^{-1}) using a "locally dense" basis DFT approach. Use of both pure (BPW91) and hybrid (B3LYP) functionals give similar results. Second, we find good agreement between predicted and experimental asymmetry parameter (η) values. Third, we find that the electric field gradient tensor orientations are consistent with those reported experimentally. Fourth, MO, spin density, and other property results are shown to help explain some interesting aspects of structure and bonding in several model metalloporphyrin systems. For example, the MOs and spin density results in the $S = {}^1/_2$ systems $[Fe(TMP)(1\text{-}MeIm)_2]^+$ and $[Fe(OEP)(t\text{-}BuNC)_2]^+$ clearly indicate the presence of different electronic configurations: $(d_{xy})^2(d_{xz},d_{yz})^3$ and $(d_{xz},d_{yz})^4(d_{xy})^1$, respectively. MO, charge, and spin density analyses of Fe(OEP)(NO) suggest a picture of an almost neutral NO moiety with the single unpaired electron mainly localized on Fe, consistent with other recent theoretical findings.[47,64,66] When taken together, these results indicate that it is now possible to quite accurately predict Mössbauer electric field gradient tensor properties (ΔE_Q, η, orientations) in both paramagnetic as well as diamagnetic heme proteins and model compounds. The ability to predict Mössbauer EFG parameters can be expected to open up a broad area of research in investigating the structures of paramagnetic metalloproteins, where very extensive experimental Mössbauer data have been reported.[14] Such capabilities should be of general use in the context of investigating the structures of paramagnetic heme proteins in particular and paramagnetic metalloproteins and metalloporphyrins in general.

Acknowledgment. This work was supported by the United States Public Health Service (NIH Grant EB 00271-24). J.M. was supported by an American Heart Association, Midwest Affiliate, Predoctoral Fellowship. Computations were carried out in part at the National Center for Supercomputing Applications (funded in part by the National Computational Science Alliance, Grants MCB-000018N, MCB-000020N, and MCB-010016N).

JA020298O